*American Mineralogist, Volume 79, pages 63–72, 1994*

# Crystal chemistry and microstructures of plutonic biotite

**Simona Bigi, Maria Franca Brigatti**
Istituto di Mineralogia e Petrografia, Università di Modena, Via S. Eufemia, 19, 41100 Modena, Italy

## Abstract

Transmission electron microscope and single-crystal X-ray diffraction studies were carried out on biotite from the Valle del Cervo plutonic body (northwestern Italy) with the aim of characterizing their structures and microstructures and also of establishing possible relationships between polytypism and crystal chemistry. The crystals, from the same lithologic complex, do not present significant chemical variations. On the other hand, they contain many different polytypic sequences, such as $1M$ and $2M_1$, which represent the most common polytypes, $3T$ and disordered and long-period stacking sequences, which often coexist in the same crystal. Four-, five-, six-, seven-, eight-, nine-, 13-, 14-, and 21-layer polytypes, often interrupted by stacking faults, were also observed.

No relationship was found between polytypic sequences and chemistry, whereas the observed microstructures seem to be related to the petrological environment. The microstructural study facilitated the interpretation of difference-Fourier maps obtained from structure refinements of biotite from the same rock samples. The crystal-chemical study of two biotite samples, $1M$ (space group $C2/m$) and $2M_1$ (space group $C2/c$), from the same rock sample and with very similar chemical composition did not reveal any substantial differences in the mean bond lengths, whereas the octahedral and tetrahedral distortion parameters are higher in $2M_1$ than in $1M$. Both polytypes exhibit M1 mean bond lengths greater than M2 mean bond lengths, suggesting partial cation ordering, whereas no tetrahedral cation ordering can be detected in the $2M_1$ polytype.

## Introduction

Biotite is widespread in igneous rocks, and its chemical and structural properties influence many important igneous reactions. Although much attention has been devoted to chemical studies of biotite, until recently there has been a paucity of crystal structure refinement data because biotite is commonly affected by stacking faults, chemical disorder, superstructures, twins, and intergrowths with other phases (Bailey, 1984). Information on microstructures can be obtained by transmission electron microscope (TEM) studies. Nevertheless, TEM studies on plutonic biotite have been mostly concerned with alteration processes (Veblen and Ferry, 1983; Eggleton and Banfield, 1985); only a few studies on metamorphic biotite, pegmatitic muscovite, and lepidolite samples have dealt with the coexistence of different polytypic sequences in the same crystal (Bell and Wilson, 1981, 1986; Rule et al., 1987).

Accordingly, the aim of this study was to characterize the crystal chemistry and the microstructures of plutonic biotite using TEM techniques [selected-area electron diffraction (SAED) and bright- and dark-field imaging] and single-crystal X-ray structure refinements of $1M$ and $2M_1$ polytypes. Crystal structure refinements on biotite-$1M$ from this plutonic complex have been previously published (Brigatti and Davoli, 1990). In the present study two new structure refinements of coexisting biotite-$1M$ and -$2M_1$ from the same rock sample and with similar chemical composition were carried out with the aim of comparing crystal-chemical variations induced only by the different polytypic arrangements.

## Sample description

The biotite samples studied came from the Valle del Cervo plutonic complex (Vercelli, northwestern Italy). Geochemical and petrological features of the Valle del Cervo area have been extensively studied, and a review is presented in Bigioggero and Tunesi (1988). The pluton, of orogenic character and shoshonitic affinity, is intruded into the pre-Alpine basement rocks of the Sesia-Lanzo Zone at the boundary of the south-Alpine Ivrea-Verbano Zone. It comprises three main lithologic complexes in a roughly concentric arrangement. The core consists mainly of granite and the rim of quartz syenite and quartz monzonite; they are named the granitic, syenitic, and monzonitic complexes, respectively.

In the granitic complex, biotite figures as a major mineral in addition to quartz, potassium feldspar, plagioclase, and sometimes hornblende; apatite, sphene, and zircon are accessory minerals. Biotite appears as coarse brown flakes and prevails over hornblende; alteration to chlorite at the rim of the grains and along cleavages is sometimes observed. In the syenitic complex, small amounts of augite also appear, although hornblende is

0003–004X/94/0102–0063$02.00

**TABLE 1.** Averaged chemical compositions and structural formulae of Valle del Cervo biotite determined by EPMA except where noted

| Sample: | M13 | M105 | M7* | | M32 | M16 | M14 | M62 |
|---|---|---|---|---|---|---|---|---|
| Polytype: | | | 1*M* | 2$M_1$ | | | | |
| | | | **Biotite chemical composition** | | | | | |
| $SiO_2$ | 37.11 | 35.70 | 36.84 | 36.44 | 37.12 | 35.94 | 36.50 | 36.25 |
| $TiO_2$ | 3.99 | 3.53 | 3.49 | 3.90 | 2.70 | 4.25 | 4.03 | 3.39 |
| $Al_2O_3$ | 13.34 | 13.99 | 13.74 | 13.51 | 13.65 | 13.55 | 13.20 | 13.90 |
| $Fe_2O_3$ | 5.86 | 6.88 | 8.77 | 8.99 | 8.06 | 9.26 | 8.39 | 6.80 |
| FeO** | 14.14 | 14.67 | 10.90 | 10.90 | 11.31 | 13.93 | 12.34 | 14.81 |
| MgO | 11.82 | 11.78 | 13.51 | 13.57 | 13.38 | 9.81 | 12.62 | 11.80 |
| MnO | 0.51 | 0.48 | 0.33 | 0.27 | 0.43 | 0.21 | 0.19 | 0.49 |
| $Li_2O$† | 0.05 | 0.02 | nd | nd | 0.04 | 0.00 | 0.03 | 0.03 |
| $Na_2O$ | 0.08 | 0.14 | 0.11 | 0.21 | 0.08 | 0.10 | 0.17 | 0.10 |
| $K_2O$ | 10.12 | 9.29 | 9.80 | 9.70 | 9.59 | 9.25 | 9.24 | 9.57 |
| CaO | 0.02 | 0.00 | 0.00 | 0.00 | 0.06 | 0.01 | 0.00 | 0.00 |
| $H_2O$‡ | 2.83 | 3.41 | 2.50 | 2.50 | 3.44 | 3.14 | 3.00 | 2.80 |
| Cl | 0.12 | 0.13 | 0.00 | 0.00 | 0.14 | 0.55 | 0.30 | 0.06 |
| Total | 99.99 | 100.02 | 99.99 | 99.99 | 100.00 | 100.00 | 100.01 | 100.00 |
| | | | **Biotite structural formulas (O + OH + Cl = 24)** | | | | | |
| Si | 5.691 | 5.456 | 5.619 | 5.568 | 5.595 | 5.527 | 5.561 | 5.581 |
| Al | 2.309 | 2.521 | 2.381 | 2.432 | 2.405 | 2.456 | 2.370 | 2.419 |
| $Fe^{3+}$ | — | 0.023 | — | — | — | 0.017 | 0.069 | — |
| Total | 8.000 | 8.000 | 8.000 | 8.000 | 8.000 | 8.000 | 8.000 | 8.000 |
| Al | 0.103 | — | 0.090 | — | 0.020 | — | — | 0.104 |
| $Fe^{3+}$ | 0.676 | 0.768 | 1.007 | 1.034 | 0.914 | 1.054 | 0.893 | 0.788 |
| $Fe^{2+}$ | 1.813 | 1.875 | 1.390 | 1.393 | 1.426 | 1.791 | 1.572 | 1.907 |
| Mg | 2.702 | 2.683 | 3.071 | 3.090 | 3.006 | 2.248 | 2.865 | 2.707 |
| Mn | 0.066 | 0.062 | 0.043 | 0.035 | 0.055 | 0.027 | 0.025 | 0.064 |
| Ti | 0.460 | 0.406 | 0.400 | 0.448 | 0.306 | 0.491 | 0.462 | 0.392 |
| Li | 0.031 | 0.012 | — | — | 0.024 | — | 0.018 | 0.019 |
| Total | 5.852 | 5.806 | 6.001 | 6.000 | 5.751 | 5.611 | 5.835 | 5.981 |
| Ca | 0.003 | — | — | — | 0.010 | 0.002 | — | — |
| Na | 0.024 | 0.041 | 0.033 | 0.062 | 0.023 | 0.030 | 0.050 | 0.030 |
| K | 1.980 | 1.811 | 1.907 | 1.891 | 1.844 | 1.815 | 1.796 | 1.880 |
| Total | 2.007 | 1.852 | 1.940 | 1.953 | 1.877 | 1.847 | 1.846 | 1.910 |
| OH | 2.895 | 3.476 | 2.544 | 2.548 | 3.459 | 2.456 | 3.049 | 2.875 |
| Cl | 0.031 | 0.034 | — | — | 0.036 | 0.143 | 0.077 | 0.016 |
| O | 21.074 | 20.490 | 21.456 | 21.452 | 20.505 | 21.401 | 20.874 | 21.109 |
| Total | 24.000 | 24.000 | 24.000 | 24.000 | 24.000 | 24.000 | 24.000 | 24.000 |

*Note:* biotite chemical compositions are given in weight percentages.
* Analyses on crystals used for structure refinements.
** The Fe oxidation state was determined by semi-microvolumetric method (Meyrowitz, 1970).
† Determined by atomic absorption spectrophotometry.
‡ Determined by thermogravimetric analysis.

the prevailing ferromagnesian mineral. Biotite can be isolated, aggregated, or included in hornblende. In the monzonitic complex, augite becomes the major ferromagnesian mineral.

Two samples from each lithologic complex were selected for TEM studies and single-crystal X-ray structure refinements: M13 and M105 from the granitic complex, M7 and M32 from the syenitic complex, M14 and M16 from the monzonitic complex, and M62 from the transition zone between the granitic and monzonitic complexes.

## Experimental techniques

### Chemical analyses

Electron probe microanalyses (EPMA) were carried out using an ARL-SEMQ electron microprobe. Operating conditions were a 15-keV accelerating voltage, a 20-nA sample current, and a 3-$\mu$m beam diameter. Data were reduced by the method of Ziebold and Ogilvie (1964), using the correction factors of Albee and Ray (1970). The biotite samples analyzed were homogeneous, and their averaged compositions are reported in Table 1. Since there was little variation in the biotite composition of any given rock sample, OH, $Fe^{2+}$, and Li were determined over a wide range of selected crystals: $H_2O$ was determined by thermogravimetric analysis (Du Pont 990 thermal analyzer, heating rate 10 °C/min) in Ar gas to prevent Fe oxidation (flow rate 30 mL/min); $Fe^{2+}$ was determined by a semi-microvolumetric method (Meyrowitz, 1970); and Li was determined by atomic absorption spectrophotometry. Structural formulae were calculated on the basis of (O + OH + Cl) = 24.

### TEM study

The biotite crystals used in the TEM study were handpicked from thin sections. In order to investigate polytypism and stacking disorder, crystals having **c*** parallel to the plane of the section were selected, prepared by Ar ion thinning techniques, mounted on Cu grids, and lightly coated with C. The TEM specimens were examined with a Philips 400T transmission electron microscope oper-

**TABLE 2.** Unit-cell parameters and details of X-ray data collection and refinement

| Sample | Dimensions (mm) | $N_{obs}$ | $R_{sym}$ (×100) | $R_{obs}$ (×100) | $a$ (Å) | $b$ (Å) | $c$ (Å) | $\beta$ (°) | $V$ (Å³) |
|---|---|---|---|---|---|---|---|---|---|
| 1*M* polytype | 0.27 × 0.24 × 0.02 | 549 | 2.31 | 3.33 | 5.335(2) | 9.244(2) | 10.206(3) | 100.08(2) | 495.6 |
| 2$M_1$ polytype | 0.15 × 0.12 × 0.02 | 724 | 2.63 | 2.72 | 5.339(1) | 9.249(1) | 20.196(1) | 95.06(1) | 993.4 |

*Note:* $R_{sym} = \left(\sum_{hkl}\sum_{i=1}^{N} |I_{hkl,i} - I_{hkl}|\right) \Big/ \left(\sum_{hkl}\sum_{i=1}^{N} I_{hkl}\right)$.

ating at 100 keV and equipped with an EDAX energy-dispersive SiLi detector. SAED patterns were used to characterize the main periodicity and ordering of the polytypic sequences and intergrowths with other phases. In mica SAED patterns obtained with the beam parallel to [100], [110], or [$\bar{1}$10], the rows with $k = 3n$ exhibit a 10-Å periodicity for every kind of sequence; the true periodicity and ordering are indicated by the distribution and shape of the spots in the rows with $k \neq 3n$. Weak spots, corresponding to forbidden reflections, sometimes appear in the [00*l*]* rows and are generated by multiple diffraction effects in the thickest areas. The main periodicity and ordering were also studied by bright- and dark-field imaging and high-resolution (HRTEM) imaging. HRTEM images were obtained by selecting the 00*l* and 02*l* reflections with the objective aperture (70-$\mu$m diameter); one-dimensional bright-field images were obtained using the 00*l* reflections and centering the objective aperture (30-$\mu$m diameter) on the transmitted beam; dark-field images were obtained using the same aperture centered about the [02*l*]* reciprocal lattice row. Superstructures were detected in thick areas of the specimens, where dynamic diffraction effects were present (Iijima and Buseck, 1978).

SAED patterns were interpreted by comparing observed and calculated diffraction patterns for [02*l*]*, [11*l*]*, and [$\bar{1}$1*l*]* reciprocal lattice rows. A periodic intensity distribution function for each complex polytype was computed following the formulae proposed by Takeda (1967).

### X-ray data collection and structure refinement

Biotite crystals, selected from crushed samples, were mounted along the **b** direction on a CAD4 (Enraf-Nonius) four-circle diffractometer with graphite-monochromatized Mo$K\alpha$ radiation, operating at 52 kV and 40 mA. The unit-cell parameters reported in Table 2 were calculated by means of least-squares refinement using 25 reflections ($15° \leq \theta \leq 25°$); technical details of data measurement and reduction have already been extensively described (Brigatti and Davoli, 1990; Brigatti et al., 1991; Bigi et al., 1993). Two equivalent sets of reflections were measured in the $\theta$ ranges 1.5–35.0° (biotite-1*M*, 2400 measured reflections) and 2.0–33.0° (biotite-2$M_1$, 3070 measured reflections) and were merged after correction for absorption (North et al., 1968) and Lorentz-polarization effects. The crystal-structure refinements were performed without chemical constraints using the least-squares program ORFLS (Busing et al., 1962). Scattering factors for fully ionized atoms were used for M1 and M2 octahedral and K interlayer sites, whereas scattering factors for neutral atoms were used for the tetrahedral and O sites. The interpretation of structural data is based on averaged *C*2/*m* and *C*2/*c* structures for 1*M* and 2$M_1$ polytypes, respectively. Crystallographic coordinates and isotropic and anisotropic temperature factors are reported in Table 3; relevant bond lengths are reported in Table 4. Observed and calculated structure factors are listed in Table 5.[1]

## CHEMISTRY

Electron probe microanalyses of Valle del Cervo biotite samples are reported in Table 1. The main chemical variation relates to the $Fe^{2+}$-Mg ratio, which ranges between 0.47 and 0.70. The $Fe^{3+}$ content is always less than that of $Fe^{2+}$. No significant chemical variations occur in different crystals from the same rock sample, and zoning is unlikely to be present. No well-defined relationships between chemistry and microstructures were observed in TEM-EDS microanalyses, since different stacking sequences coexisting in the same crystal have very similar chemical compositions. Only in sample M7 is there a weak relationship between the Fe content and polytypism, the 1*M* polytype being enriched in Fe with respect to 2$M_1$ and 3*T*; but that can be ascribed to local environmental chemical variations occurring during crystal growth.

## MICROSTRUCTURES

Weissenberg and precession photographs emphasized that Valle del Cervo biotite is mostly characterized by 1*M*, 2$M_1$, and disordered polytypes. TEM study showed that ordered 1*M*, 2$M_1$, and 3*T* sequences can extend over large areas of the crystal, whereas disorder is characterized by the coexistence of different microstructures, namely, ordered, simple, and complex polytypes, twinnings, completely disordered stacking sequences, and intergrowths of 14-Å phases. These sequences can occur in areas comprising a few nanometers to a few micrometers, producing a patchwork of microstructures. Also, the simple polytypes are often interrupted by isolated stacking

[1] A copy of Table 5 may be ordered as Document AM-94-543 from the Business Office, Mineralogical Society of America, 1130 Seventeenth Street NW, Suite 330, Washington, DC 20036, U.S.A. Please remit $5.00 in advance for the microfiche.

**TABLE 3.** Crystallographic coordinates and equivalent isotropic (Å$^3$) and anisotropic temperature factors (Å$^3$ × 10$^4$)

| Atom | x/a | y/b | z/c | $B_{eq}$ | $\beta_{11}$ | $\beta_{22}$ | $\beta_{33}$ | $\beta_{12}$ | $\beta_{13}$ | $\beta_{23}$ |
|---|---|---|---|---|---|---|---|---|---|---|
| | | | | | **1*M* polytype** | | | | | |
| O1 | 0.0247(8) | 0 | 0.1688(4) | 2.6(1) | 306(16) | 47(4) | 71(5) | 0 | 21(7) | 0 |
| O2 | 0.3219(5) | 0.2336(3) | 0.1683(3) | 2.64(7) | 212(9) | 88(4) | 66(3) | −22(5) | 34(4) | −6(3) |
| O3 | 0.1334(4) | 0.1675(3) | 0.3905(3) | 2.01(6) | 197(8) | 44(2) | 61(3) | 0(4) | 29(4) | 4(3) |
| O4 | 0.1301(7) | ½ | 0.3952(4) | 2.17(9) | 198(13) | 53(4) | 64(4) | 0 | 27(6) | 0 |
| M1 | 0 | 0 | ½ | 1.92(4) | 172(5) | 38(2) | 67(2) | 0 | 36(3) | 0 |
| M2 | 0 | 0.3343(1) | ½ | 1.86(2) | 160(4) | 44(1) | 60(1) | 0 | 28(2) | 0 |
| K | 0 | ½ | 0 | 3.65(6) | 339(9) | 87(3) | 107(3) | 0 | 42(4) | 0 |
| T | 0.0752(2) | 0.1669(1) | 0.2258(1) | 1.71(2) | 161(3) | 38(1) | 52(1) | −2(2) | 21(1) | 1(1) |
| | | | | | **2$M_1$ polytype** | | | | | |
| O11 | 0.7385(6) | 0.3176(4) | 0.1656(2) | 1.64(8) | 129(12) | 51(4) | 11(1) | −15(6) | 4(3) | −1(2) |
| O21 | 0.2368(6) | 0.3478(4) | 0.1665(2) | 1.62(8) | 143(12) | 44(4) | 11(1) | 10(6) | 0(3) | −1(2) |
| O22 | 0.4418(5) | 0.0844(4) | 0.1662(1) | 1.66(6) | 165(10) | 38(3) | 11(1) | 7(7) | 7(2) | −3(2) |
| O31 | 0.4324(5) | 0.2376(3) | 0.0550(1) | 0.63(6) | 82(9) | 6(3) | 5(1) | −2(4) | 0(2) | −1(1) |
| O32 | 0.9359(5) | 0.4047(3) | 0.0550(1) | 0.95(6) | 98(9) | 22(3) | 6(1) | 2(5) | 4(2) | −2(1) |
| O4 | 0.9351(5) | 0.0695(3) | 0.0518(1) | 1.08(6) | 103(9) | 19(3) | 9(1) | 10(5) | 5(2) | −5(1) |
| M1 | ¾ | ¼ | 0 | 1.04(3) | 69(4) | 31(1) | 8(1) | −8(4) | 3(1) | −4(1) |
| M2 | 0.2473(2) | 0.0825(1) | 0.0000(1) | 1.22(2) | 112(3) | 33(1) | 8(1) | −3(5) | 4(1) | −3(1) |
| K | 0 | 0.0852(3) | ¼ | 2.93(4) | 238(5) | 81(2) | 21(1) | 0 | 7(1) | 0 |
| T1 | 0.4615(2) | 0.2498(1) | 0.1370(1) | 0.89(2) | 74(3) | 23(1) | 7(1) | 3(3) | 2(1) | 1(1) |
| T2 | 0.9636(2) | 0.4166(2) | 0.1371(1) | 0.91(2) | 76(3) | 24(1) | 7(1) | 5(4) | 2(1) | 1(1) |

*Note:* anisotropic temperature factors, $\beta_{ij}$, are of the form $\exp[-(h^2\beta_{11} + \ldots + 2hk\beta_{12} + \ldots)]$.

faults, giving rise to weakly disordered sequences. The distribution of the stacking sequences in biotite from the different rock samples is reported in Table 6.

### Simple polytypes and twinnings

In biotite from the granitic and syenitic complexes, the 1*M* polytype prevails, whereas in biotite from the monzonitic complex, the 2$M_1$ polytype is the most common layer sequence. Both polytypes commonly contain stacking faults, as indicated by weak streaking along **c*** of the spots with $k \neq 3n$ (Fig. 1). It is unusual in biotite from the syenitic complex that 1*M*, 2$M_1$, and 3*T* polytypes that are almost ordered and exhibit crystallographically controlled orientations coexist in the same crystal (sample M7). Twinned sequences were found only in granitic complex biotite (Fig. 2) and consist of lamellae of the 1*M* polytype approximately 100 Å wide alternating with two orientations, which follow the most common twin laws reported by Smith and Yoder (1956). Twin lamellae coexist with disordered sequences and a dominant 1*M* polytype. Figure 2a illustrates two distinct 1*M* polytype patterns, depending on the orientation of the lamellae. Those viewed along the [1$\bar{1}$0] axis are wider and are represented by the stronger spots in rows with $k \neq 3n$. Those viewed along the [$\bar{1}$00] axis are less abundant and are represented by the weaker spots in the same rows. The corresponding twinning laws may be [110] (or [1$\bar{1}$0]) and [310] (or [3$\bar{1}$0]), produced by ±60 and ±120° layer rotations around **c***. Figure 2b shows twinning around the [110] (or [1$\bar{1}$0]) axis, or the [100] axis, or both, corresponding to ±60 and ±180° layer rotations around **c***, which is uncommon in biotite.

**TABLE 4.** Selected bond lengths (Å) from structure refinements of biotite-1*M* and -2$M_1$ samples from Valle del Cervo syenitic complex*

| | | | | | |
|---|---|---|---|---|---|
| | | | **1*M* polytype** | | |
| M1-O3 (× 4) | 2.105(2) | T-O1 | 1.654(2) | K-O1 (× 2) | 3.019(4) |
| M1-O4 (× 2) | 2.074(4) | T-O2 | 1.652(3) | K-O2 (× 4) | 3.015(3) |
| ⟨M1-O⟩ | 2.095 | T-O2′ | 1.655(3) | $\langle K\text{-}O\rangle_{inner}$ | 3.016 |
| M2-O3 (× 2) | 2.100(3) | T-O3 | 1.655(3) | | |
| M2-O3′ (× 2) | 2.076(2) | ⟨T-O⟩ | 1.654 | K-O1′ (× 2) | 3.305(4) |
| M2-O4 (× 2) | 2.057(3) | | | K-O2′ (× 4) | 3.306(3) |
| ⟨M2-O⟩ | 2.078 | | | $\langle K\text{-}O\rangle_{outer}$ | 3.306 |
| | | | **2$M_1$ polytype** | | |
| M1-O31 (× 2) | 2.111(3) | T1-O11 | 1.662(4) | K-O11 (× 2) | 3.010(4) |
| M1-O32 (× 2) | 2.018(3) | T1-O21 | 1.656(4) | K-O21 (× 2) | 3.036(4) |
| M1-O4 (× 2) | 2.163(3) | T1-O22 | 1.646(4) | K-O22 (× 2) | 3.022(3) |
| ⟨M1-O⟩ | 2.097 | T1-O31 | 1.652(3) | $\langle K\text{-}O\rangle_{inner}$ | 3.023 |
| | | ⟨T1-O⟩ | 1.654 | | |
| M2-O31 | 2.019(3) | | | K-O11′ (× 2) | 3.322(4) |
| M2-O31′ | 2.177(3) | T2-O11 | 1.654(4) | K-O21′ (× 2) | 3.274(4) |
| M2-O32 | 2.108(3) | T2-O21 | 1.653(4) | K-O22′ (× 2) | 3.295(3) |
| M2-O32′ | 2.181(3) | T2-O22 | 1.668(4) | $\langle K\text{-}O\rangle_{outer}$ | 3.297 |
| M2-O4 | 1.960(3) | T2-O32 | 1.653(3) | | |
| M2-O4′ | 2.048(3) | ⟨T2-O⟩ | 1.657 | | |
| ⟨M2-O⟩ | 2.082 | | | | |

* Sample M7.

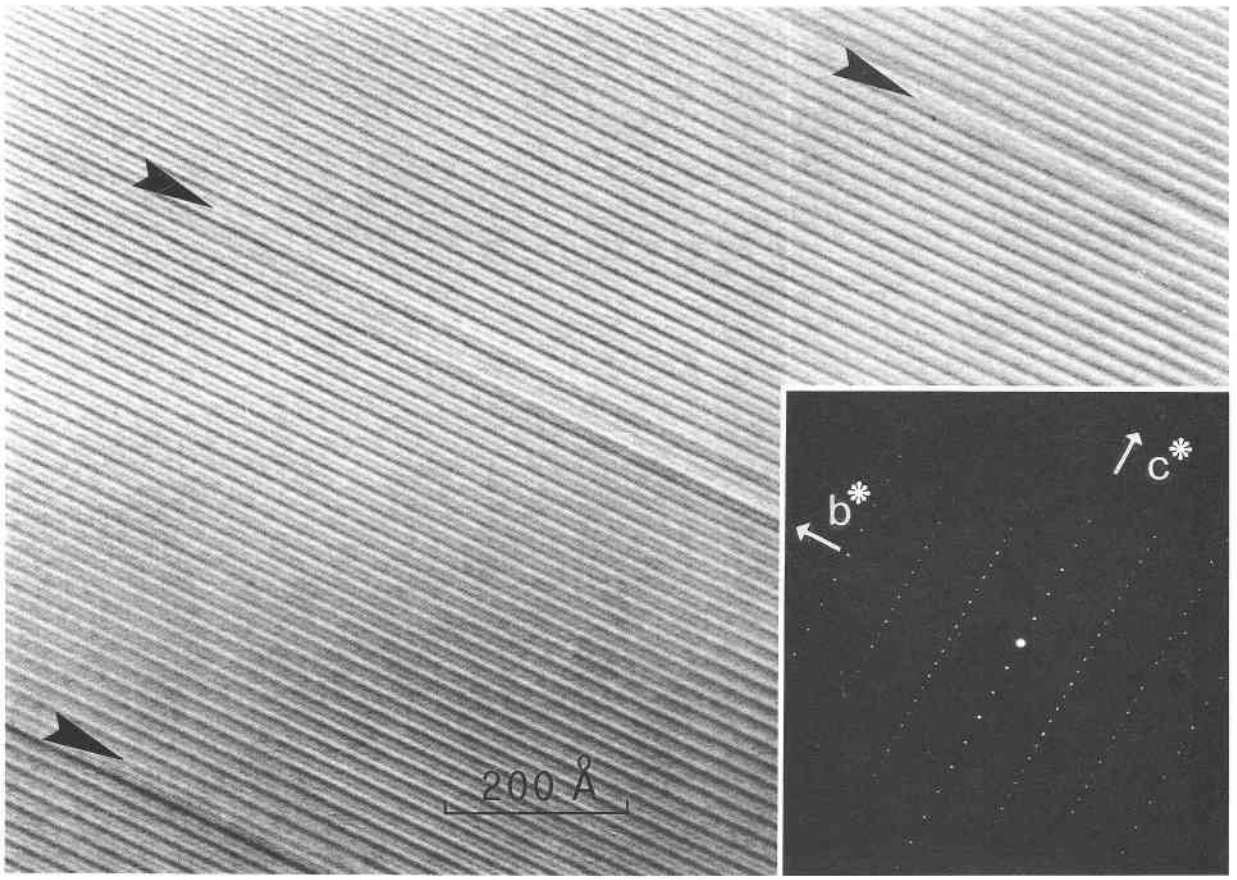


Fig. 1. HRTEM image and electron diffraction pattern of a $2M_1$ sequence affected only by a few stacking faults, as indicated by arrows. Sample M16 from the monzonitic complex.

### Long-period stacking sequences

Long-period stacking sequences are less common than the simple polytypes described above. They occur in biotite from the granitic and monzonitic complexes and in biotite from the transition zone between them, whereas they are absent in biotite from the syenitic complex. These long-period stacking sequences are easily identified by means of SAED patterns, i.e., they repeat quite regularly over an area of about 0.5 $\mu$m in diameter, which is the size of the selected-area aperture used in this work. The bright- and dark-field one-dimensional images showed that the stacking sequences are sometimes periodic for a great number of unit cells or can be interrupted by frequent stacking faults, giving rise to complex sequences with a dominant, but inconsistent, periodicity. Only in certain cases was it possible to determine the exact stacking sequence by interpreting the intensity distribution of the spots in the SAED patterns and the HRTEM images. This enabled us to describe new complex polytypes, which hitherto had only been described in theoretical terms. In granitic complex biotite, long-period stacking sequences are widely ordered and coexist with disordered sequences and simple $1M$ and $2M_1$ polytypes. Unusual superstructures were observed in sample M13. Sequences with two-, three-, nine-, and 14-layer periodicities follow one another (Fig. 3); the nature of the lamellar interfaces is sometimes characterized by disordered sequences or cleavage planes, which are often difficult to recognize because they have been damaged by ion thinning. Another area of the same crystal shows five- (Fig. 4) and 13-layer polytypes. The HRTEM image and the intensity distribution of the spots in the SAED pattern indicate that the five-layer

**TABLE 6.** Distribution of simple and complex polytypes in biotite from Valle del Cervo pluton

| Sample | Rock type | Simple polytypes | Complex polytypes (no. of layers) |
|---|---|---|---|
| M13 | Granitic complex | $1M$, $2M_1$, $3T$ | 3, 5, 9, 13, 14 |
| M105 | Granitic complex | $1M$ | |
| M14 | Monzonitic complex | $2M_1$, $1M$ | 21 |
| M16 | Monzonitic complex | $2M_1$, $1M$ | 8 |
| M7 | Syenitic complex | $1M$, $2M_1$, $3T$ | |
| M32 | Syenitic complex | $1M$ | |
| M62 | Monzonitic-syenitic complex transition zone | $1M$, $2M_1$ | 3, 4, 6, 7 |

*Note:* polytypes are indicated in decreasing order of importance.

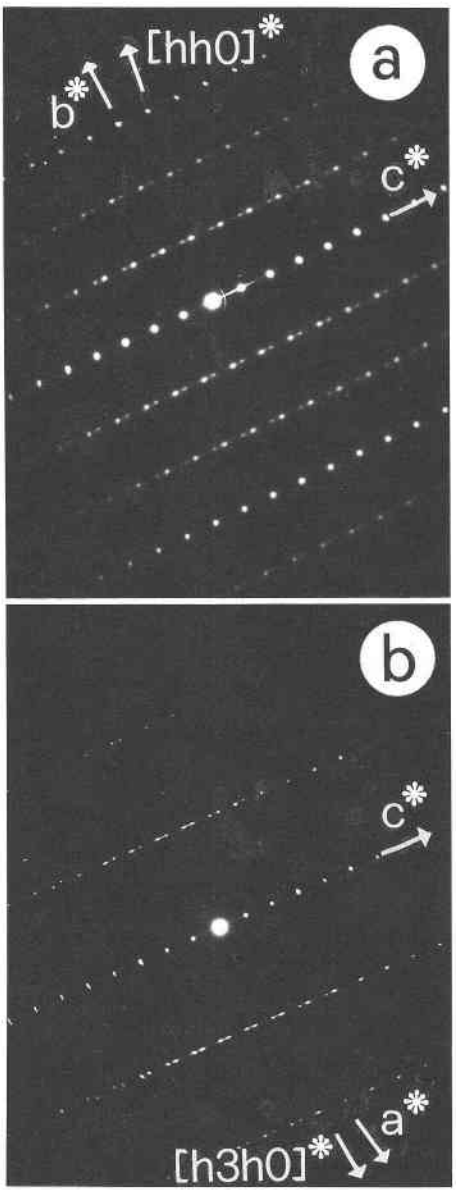


Fig. 2. Electron diffraction patterns of twinned 1*M* polytype. Twin laws: [110] (or [1$\bar{1}$0]) or [310] (or [3$\bar{1}$0]) axes (**a**) and [110] (or [1$\bar{1}$0]) or [100] axes (**b**). Sample M105 from the granitic complex.

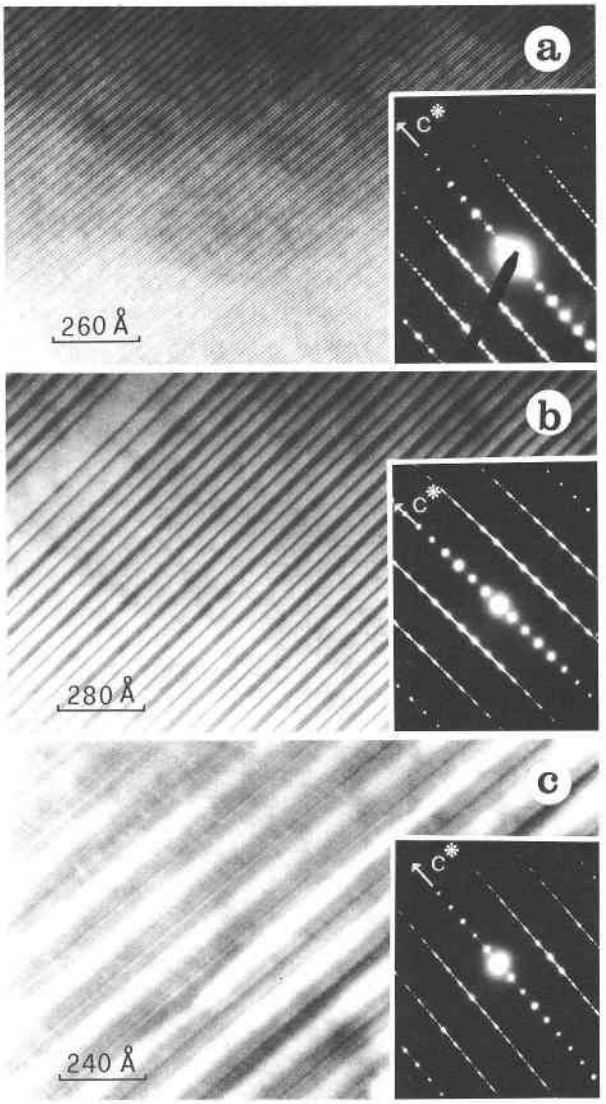


Fig. 3. Bright-field image and electron diffraction pattern of three-layer polytype (**a**), nine-layer polytype (**b**), and 14-layer polytype (**c**). The viewing direction is parallel to [100] or [110] or [$\bar{1}$10]. Sample M13 from the granitic complex.

sequence can be attributed to the complex polytype 0002$\bar{2}$, synthetically written $(0)_3 2\bar{2}$, using the RTW notation of Ross et al. (1966).

In the monzonitic complex biotite, eight- and 21-layer sequences were observed near disordered sequences; they too were often interrupted by stacking faults (Fig. 5). The complex sequences can be ascribed to the complex polytypes 00202$\bar{0}$2$\bar{2}$ and $(\bar{2}2)_4(2\bar{2})_5 222$, respectively. Complex sequences of three, four, six, and seven layers were also found in biotite from the transition zone between the granitic and monzonitic complexes (Fig. 6); they coexist in the same crystal with dominant 1*M*, $2M_1$, and 1*Md* polytypes.

## Crystal chemistry

### Preamble

Brigatti and Davoli (1990), in their biotite-1*M* structure refinements on five crystals from the three main lithologic complexes of Valle del Cervo pluton (sample M13, M14, M32, M62, M73), showed that (1) differences in bond lengths and distortion parameters exist between M1 and M2 sites because of partial cation ordering, the greatest differences being found in monzonitic complex biotite; (2) bond lengths and distortion of the octahedral sheet are influenced not only by the local chemical composition

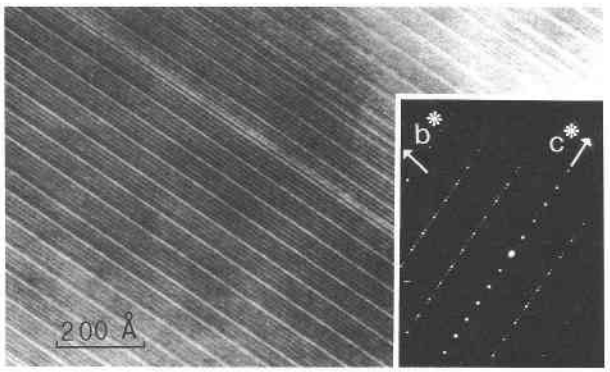


Fig. 4. Bright-field image and electron diffraction pattern of five-layer polytype. Sample M13 from the granitic complex.

but also by confinement of the octahedra between two opposing tetrahedral sheets; (3) almost regular tetrahedra are linked in pseudohexagonal rings, whose distortion from hexagonality ($\alpha$ angle, $5.3° \leq \alpha \leq 7.4°$) seems to be independent of octahedral features; and (4) difference-Fourier map analysis reveals significant peaks, suggesting two different orientations of OH groups in samples from different complexes.

### X-ray analyses and structure refinements of M7 biotite (1*M* and $2M_1$ polytypes)

The crystal-chemical relationships of biotite-1*M* and -$2M_1$ from the syenitic complex are discussed and compared with those of other biotite samples from the same plutonic body. Bond lengths are given in Table 4, and additional structural parameters compared with those reported by Brigatti and Davoli (1990) are given in Table 7.

The two studied biotite samples are of very similar

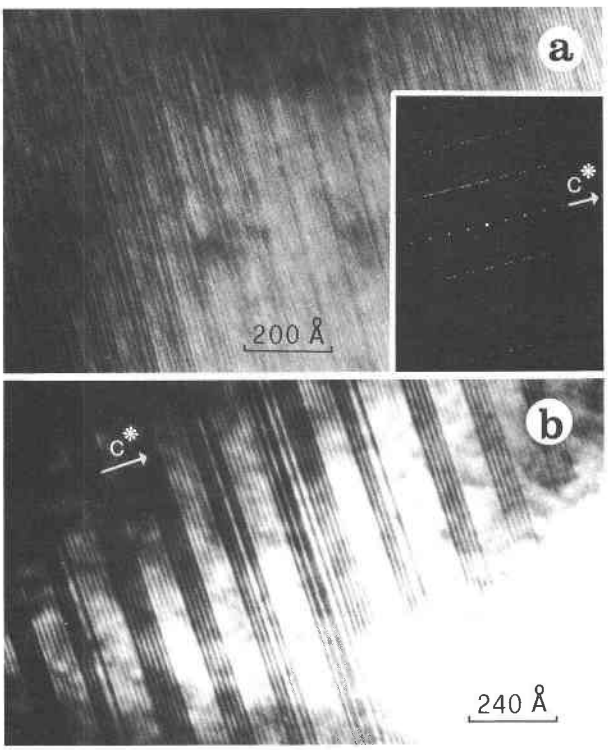


Fig. 5. Dark-field image and electron diffraction pattern of eight-layer polytype (**a**) and bright-field image of 21-layer polytype (**b**). The viewing direction is parallel to [100] or [110] or [$\bar{1}$10]. Sample M16 from the monzonitic complex.

chemical composition (Table 1). The greatest variability (little more than 10%) was observed for the $TiO_2$ content.

**Octahedral sheet.** Mean bond lengths are greater for the M1 than for the M2 site, which indicates that large

**TABLE 7.** Octahedral, tetrahedral, and interlayer parameters derived from structure refinement

| Sample: | M13 | M7 | M7 | M32 | M14 | M62 |
|---|---|---|---|---|---|---|
| Polytype: | 1*M* | 1*M* | $2M_1$ | 1*M* | 1*M* | 1*M* |
| $\beta_{ideal}$ (°) | 100.03 | 100.04 | 95.06 | 100.02 | 100.03 | 100.03 |
| $\beta_{obs}$ (°) | 100.15(3) | 100.08(2) | 95.06(1) | 100.02(3) | 100.26(2) | 100.15(2) |
| ⟨M1-O⟩ (Å) | 2.096 | 2.095 | 2.097 | 2.092 | 2.095 | 2.089 |
| ⟨M2-O⟩ (Å) | 2.081 | 2.078 | 2.082 | 2.080 | 2.077 | 2.079 |
| $OQE_{M1}$ | 1.0110 | 1.0106 | 1.0121 | 1.0107 | 1.0114 | 1.0103 |
| $OQE_{M2}$ | 1.0097 | 1.0091 | 1.0133 | 1.0098 | 1.0099 | 1.0096 |
| $\psi_{M1}$ (°) | 58.9 | 58.8 | 58.8 | 58.9 | 59.0 | 58.8 |
| $\psi_{M2}$ (°) | 58.7 | 58.5 | 58.6 | 58.7 | 58.7 | 58.6 |
| $e_o/e_{sM1}$ | 1.1055 | 1.1032 | 1.0994 | 1.1041 | 1.1073 | 1.1024 |
| $e_o/e_{sM2}$ | 1.0988 | 1.0958 | 1.0936 | 1.0992 | 1.0996 | 1.0982 |
| $V_{M1}$ | 12.07 | 12.07 | 12.09 | 12.02 | 12.05 | 11.96 |
| $V_{M2}$ | 11.84 | 11.80 | 11.83 | 11.83 | 11.77 | 11.82 |
| ⟨T1-O⟩ (Å) | 1.663 | 1.654 | 1.654 | 1.657 | 1.657 | 1.654 |
| ⟨T2-O⟩ (Å) | | | 1.657 | | | |
| $TQE_{T1}$ | 1.0006 | 1.0003 | 1.0016 | 1.0003 | 1.0003 | 1.0002 |
| $TQE_{T2}$ | | | 1.0016 | | | |
| $\tau_{T1}$ (°) | 110.6 | 110.4 | 110.7 | 110.4 | 110.4 | 110.3 |
| $\tau_{T2}$ (°) | | | 110.6 | | | |
| $\alpha$ (°) | 5.7 | 6.4 | 6.0 | 6.4 | 5.7 | 6.3 |
| $\langle K\text{-}O\rangle_{inner}$ (Å) | 3.029 | 3.016 | 3.023 | 3.026 | 3.037 | 3.020 |
| $\langle K\text{-}O\rangle_{outer}$ (Å) | 3.308 | 3.306 | 3.297 | 3.316 | 3.294 | 3.306 |

*Note:* T1 = tetrahedron T1 in $2M_1$ setting and tetrahedron T in 1*M* setting. Sample M7: this study; samples M13, M14, M32, M62: from Brigatti and Davoli (1990).

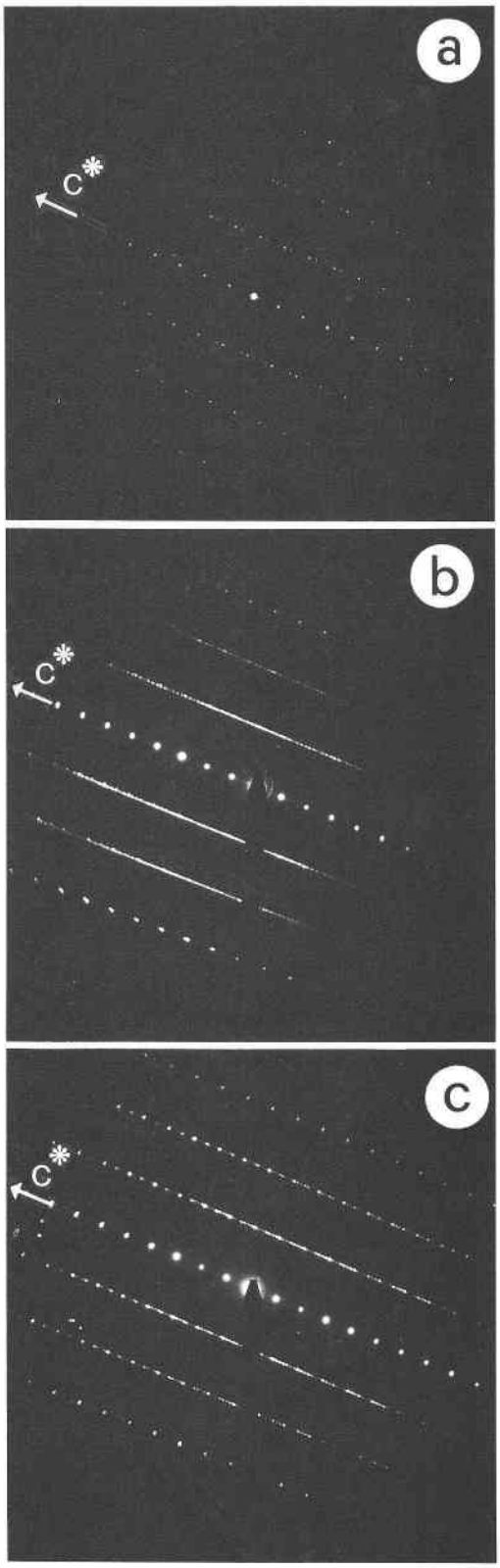


Fig. 6. Electron diffraction patterns of four-layer polytype (**a**), six-layer polytype (**b**), and seven-layer polytype (**c**). The viewing direction is parallel to [100] or [110] or [$\bar{1}$10]. Sample M62 from transition zone between the granitic and monzonitic complexes.

**TABLE 8.** Mean atomic number of octahedral and interlayer sites and determination of Al in tetrahedral sites

| | $1M$ | $2M_1$ |
|---|---|---|
| M1 Xref | 19.04 | 18.75 |
| M2 Xref | 18.10 | 18.26 |
| (M1 + 2 × M2) Xref | 55.24 | 55.27 |
| (M1 + 2 × M2) EPMA* | 55.11 | 55.45 |
| K Xref | 17.97 | 18.81 |
| K EPMA | 18.29 | 18.31 |
| $Al_{T1}$** | | 33.49 |
| $Al_{T2}$** | | 34.33 |
| $Al_T$** | 31.89 | 33.91 |
| $Al_T$ EPMA | 29.76 | 30.40 |

*Note:* Xref = X-ray refinement; EPMA = electron probe microanalyses; K = interlayer site.
* Sum of octahedral cation electrons.
** Determined by Alberti and Gottardi's (1988) method.

cations and vacancies prefer the M1 site. Both polytypes have similar mean bond lengths and mean atomic numbers (Table 8), whereas the polyhedra are more distorted in the $2M_1$ than in the $1M$ polytype (see OQE values, where OQE is the octahedral quadratic elongation, cf. Robinson et al., 1971; Table 7). At constant polyhedral volume, the distortion is caused by an increase in M1-O4, M2-O31′, and M2-O32′ and a decrease in M1-O32, M2-O31, and M2-O4 individual bond lengths (Fig. 7). As already observed by Takeda and Ross (1975), this behavior produces a shift along **b** of the triad of the upper O atoms with respect to the triad of the lower O atoms in the $2M_1$ polytype. In Figure 7, the M-O3 and M-O4 bond lengths of sample M7 are compared with those of other biotite-$1M$ and -$2M_1$ structure refinements from the literature. In the $1M$ polytype the mean bond length ⟨M1-O3⟩ increases as M1-O4 increases, whereas in the $2M_1$ polytype the ⟨M1-O3⟩ mean bond length increases as ⟨M1-O4⟩ decreases. No well-defined correlation exists for the M2 site. Thus, the octahedral-sheet geometrical variations seem mostly due to an increase in the M1 site dimension in the $1M$ polytype and to an increase in the distortion, mostly of the M1 site, in the $2M_1$ polytype.

**Tetrahedral and interlayer sheets.** The mean bond lengths ⟨T1-O⟩ and ⟨T2-O⟩ for the biotite-$2M_1$ are very similar, suggesting no $^{[4]}$Al ordering. Tetrahedral and interlayer parameters (i.e., $\alpha$, $\langle K\text{-}O\rangle_{inner}$ and $\langle K\text{-}O\rangle_{outer}$) of $1M$ and $2M_1$ polytypes are comparable. The only, albeit limited, variation concerns the TQE parameter (tetrahedral quadratic elongation: Robinson et al., 1971), which is greater in the $2M_1$ than in the $1M$ polytype. The tetrahedral deformation is caused by a decrease in the O22-T1-O31 angle (107.01°) and an increase in the O22-T2-O32 angle (114.4°) with respect to the ideal value of

109.47°. Similarly T1-O22 is significantly shorter, and T1-O11 is significantly longer.

**Difference-Fourier maps and microstructures.** A difference-Fourier map calculated at the end of anisotropic refinement affords useful information. However, care must be exercised in its interpretation, since some peaks, especially in micas, can be ascribed to artifacts linked to systematic errors or to poorly described thermal ellipsoids.

The standard deviations for the estimation of electron density using the equation of Lipson and Cochran (1953) were 0.06 (for the $2M_1$ polytype) and between 0.04 and 0.08 e/Å$^3$ (for $1M$ polytypes: samples from this study and Brigatti and Davoli, 1990).

In sample M7 the $2M_1$ polytype exhibits 18 peaks above the background ($3\sigma$). Of these, only one peak (0.26 e/Å$^3$) was found in a position suitable for H, though the distance H-O4 is somewhat short (0.86 Å). On the other hand, the $1M$ polytype exhibits peaks (about $5\sigma$) in positions corresponding to a shift of $+\mathbf{b}/3$ for T atoms and $\pm\mathbf{b}/3$ for K. Similar peaks were observed also in difference-Fourier maps of biotite from the granitic complex (M13) and from the transition zone between the syenitic and monzonitic complexes (M62). These features may be explained by twinning about [310] (or [3$\bar{1}$0]), or by $2M_1$ domains in a $1M$ sequence. TEM analyses on crystals from the same rock samples indicated that the $\mathbf{b}/3$ shift can be attributed mainly to twinning in the granitic biotite and prevalently to $2M_1$ coexisting domains in biotite from the other complexes.

## Conclusions

Comparison between biotite-$1M$ and -$2M_1$ from the Valle del Cervo syenitic complex reveals similar chemical composition and similar crystal-chemical features. The differences mostly concern the distortion parameters of both tetrahedral and octahedral polyhedra. This behavior extends the conclusions of Takeda and Ross (1975) regarding the volcanic biotite to the plutonic environment.

The microstructural study shows the existence in the same crystal of extensive areas characterized by ordered simple sequences, mostly belonging to the $1M$ polytype, variably ordered complex sequences, and disorder. The distribution of layer sequences in the biotite can be roughly related to different lithotypes: the $2M_1$ polytype is more diffuse in crystals from the monzonitic complex and twinned sequences are present only in crystals from the granitic complex, whereas long-period stacking sequences are found in biotite from both granitic and monzonitic complexes and in the transition zone between them. Syenitic complex biotite is characterized by simple ordered polytypes, sometimes coexisting in the same crystal, or by completely disordered stacking sequences ($1Md$). Furthermore, no evident correlations were found between different polytypic arrangements and chemical composition, which supports the claims in the literature for poor chemical control over polytypism; small differences between the Fe-Mg ratios of the $1M$ and $2M_1$ sequences can be ascribed to the local chemical environment.

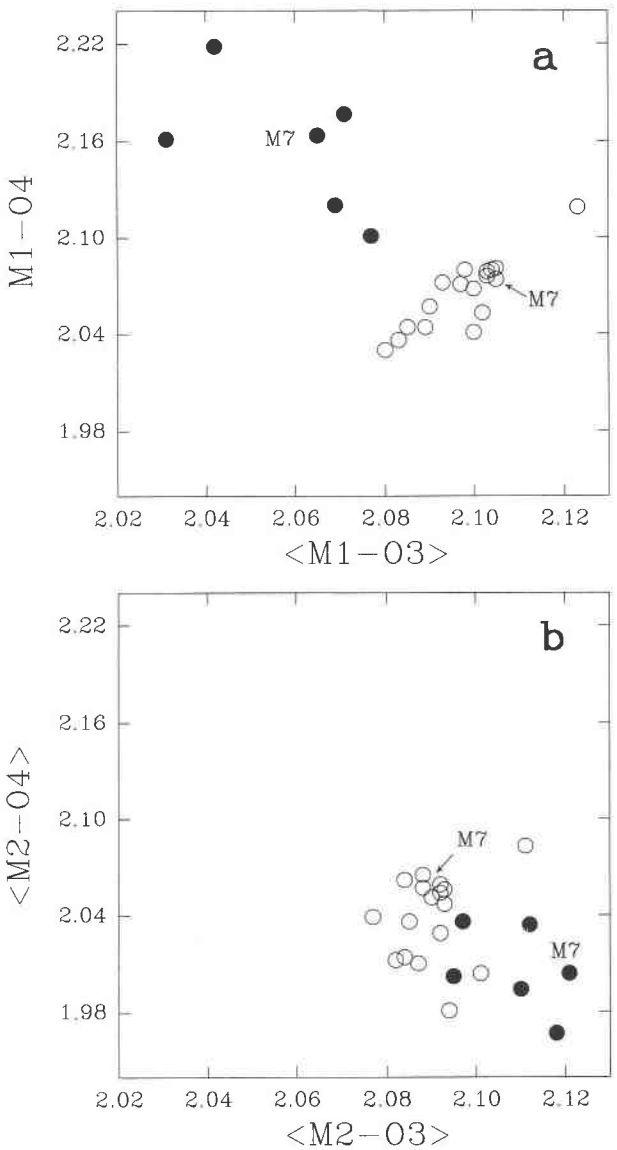


Fig. 7. Plots of ⟨M1-O3⟩ (Å) vs. M1-O4 (Å) (**a**) and ⟨M2-O3⟩ (Å) vs. ⟨M2-O4⟩ (Å); (**b**) mean bond lengths for biotite-$1M$ (open circles) and -$2M_1$ (solid circles). The samples from literature are from Brigatti and Davoli (1990); Brigatti et al. (1991); Takeda and Ross (1975); Bohlen et al. (1980).

Long-period stacking sequences in the Valle del Cervo biotite have high statistical significance (Veblen and Buseck, 1979) and are therefore useful indicators of mechanisms acting during crystal growth. Theories explaining the origin of polytypism in layered compounds falls into two main categories: kinetic and structural. In micas, on the basis of experimental studies, the kinetic theory seems to prevail; ordered long-period sequences can, in fact, be generated in an ordered simple sequence by screw dislocation, followed by spiral growth (Baronnet, 1980). However, this mechanism cannot explain the origin of partially disordered long-period sequences, and other

mechanisms involving long-range interactions must be invoked accordingly.

## Acknowledgments

We would like to thank S. Merlino for his critical reading of the manuscript; A. Gregnanin and B. Biggioggero, who supplied samples, are also acknowledged.

Financial support was provided by the Centro di Calcolo and Centro Strumenti of Modena University, the Ministero della Ricerca Scientifica e Tecnologica, and the Consiglio Nazionale delle Ricerche of Italy. The Consiglio Nazionale delle Ricerche is also acknowledged for financing the electron microprobe laboratory in Modena University.

## References cited

Albee, A.L., and Ray, L. (1970) Correction factors for electron microanalysis of silicates, oxides, carbonates, phosphates and sulphates. Analytical Chemistry, 42, 1408–1414.

Alberti, A., and Gottardi, G. (1988) The determination of the Al-content in the tetrahedra of framework silicates. Zeitschrift für Kristallographie, 184, 49–61.

Bailey, S.W. (1984) Crystal chemistry of the true micas. In Mineralogical Society of America Reviews in Mineralogy, 13, 13–60.

Baronnet, A. (1980) Polytypism in micas: A survey with emphasis on the crystal growth aspect. Current Topics in Material of Science, 5, 447–548.

Bell, I.A., and Wilson, C.J.L. (1981) Deformation of biotite and muscovite: TEM microstructures and deformation model. Tectonophysics, 78, 201–228.

——— (1986) TEM observations of defects in biotite and their relationship to polytypism. Bulletin de Minéralogie, 109, 163–170.

Bigi, S., Brigatti, M.F., Mazzucchelli, M., and Rivalenti, G. (1993) Crystal chemical variations in Ba-rich biotites from gabbroic rocks of lower crust (Ivrea Zone, N.W. Italy). Contributions to Mineralogy and Petrology, 113, 87–99.

Bigioggero, B., and Tunesi, A. (1988) The "Valle del Cervo" plutonic body. Notes to the field trip on 1st October 1987. Rendiconti della Societá Italiana di Mineralogia e Petrografia, 43, 355–366.

Bohlen, S.R., Peacor, D.R., and Essene, E.J. (1980) Crystal chemistry of a metamorphic biotite and its significance in water barometry. American Mineralogist, 65, 55–62.

Brigatti, M.F., and Davoli, P. (1990) Crystal-structure refinements of 1*M* plutonic biotites. American Mineralogist, 75, 305–313.

Brigatti, M.F., Galli, E., and Poppi, L. (1991) Effect of Ti substitution in biotite-1*M* crystal chemistry. American Mineralogist, 76, 1174–1183.

Busing, W.R., Martin, K.O., and Levi, H.S. (1962) ORFLS, a Fortran crystallographic least-squares program. U.S. National Technical Information Section, ORNL-TM-305.

Eggleton, R.A., and Banfield, J.F. (1985) The alteration of granitic biotite to chlorite. American Mineralogist, 70, 902–910.

Iijima, S., and Buseck, P.R. (1978) Experimental study of disordered mica structures by high-resolution electron microscopy. Acta Crystallographica, A34, 709–719.

Lipson, H., and Cochran, W. (1953) The crystalline state, vol. III. The determination of crystal structures, 345 p. Bell, London.

Meyrowitz, R. (1970) New semimicroprocedure for determination of ferrous iron in refractory silicate minerals using a sodium metafluoborate decomposition. Analytical Chemistry, 42, 1110–1113.

North, A.C.T., Phillips, D.C., and Mathews, F.S. (1968) Semi-empirical method of absorption correction. Acta Crystallographica, A24, 351–359.

Robinson, K., Gibbs, G.V., and Ribbe, P.H. (1971) Quadratic elongation: A quantitative measure of distortion in coordination polyhedra. Science, 172, 567–570.

Ross, M., Takeda, H., and Wones, D.R. (1966) Mica polytypes: Systematic description and identification. Science, 151, 191–193.

Rule, A.C., Bailey, S.W., Livi, K.J.T., and Veblen, D.R. (1987) Complex stacking sequences in a lepidolite from Tordal, Norway. American Mineralogist, 72, 1163–1169.

Smith, J.V., and Yoder, H.S. (1956) Experimental and theoretical studies of the mica polymorphs. Mineralogical Magazine, 31, 209–235.

Takeda, H. (1967) Determination of layer stacking sequence of a new complex mica polytype: A 4-layer lithium fluorophlogopite. Acta Crystallographica, 22, 845–853.

Takeda, H., and Ross, M. (1975) Mica polytypism: Dissimilarities in the crystal structures of coexisting 1*M* and $2M_1$ biotite. American Mineralogist, 60, 1030–1040.

Veblen, D.R., and Buseck, P.R. (1979) Chain-width order and disorder in biopyriboles. American Mineralogist, 64, 687–700.

Veblen, D.R., and Ferry, J.M. (1983) A TEM study of the biotite-chlorite reaction and comparison with petrologic observations. American Mineralogist, 68, 1160–1168.

Ziebold, T.O., and Ogilvie, R.E. (1964) An empirical method for electron microanalysis. Analytical Chemistry, 36, 322–327.

Manuscript received December 22, 1992
Manuscript accepted September 3, 1993